Chemical Science

ROYAL SOCIETY OF CHEMISTRY

EDGE ARTICLE

View Article Online
View Journal | View Issue

Cite this: *Chem. Sci.*, 2022, **13**, 6882

All publication charges for this article have been paid for by the Royal Society of Chemistry

Received 2nd April 2022
Accepted 17th May 2022

DOI: 10.1039/d2sc01922a

rsc.li/chemical-science

Control of photoluminescence quantum yield and long-lived triplet emission lifetime in organic alloys†

Zhen Xu, ‡ Duane Hean, ‡ Jennifer Yuan and Michael O. Wolf *

Two-component crystalline organic alloys with a wide range of compositional ratios (from 30% to 90% of one component) are employed to tune excited-state lifetimes and photoluminescence quantum yields (PLQYs). Alloy crystals exhibit homogeneous distribution of parent compounds by X-ray crystallography and differential scanning calorimetry. The alloys display a 1.5- to 5-fold enhancement in thermally activated delayed fluorescence (TADF) lifetime, compared to the parent compounds. PLQYs can also be tuned by changing alloy composition. The reverse intersystem crossing and long-lived lifetime of the parent compounds give rise to long-lived TADF in the alloys. Organic alloys enable tunability of both lifetime and efficiency, providing a new perspective on the development of organic long-lived emissive materials beyond the rules established for host–guest doped systems.

Introduction

Organic luminescent materials in which triplet excitons are effectively utilized are desired for numerous applications, including organic light-emitting diode (OLED) displays, anti-counterfeiting inks, photodynamic therapy, chemical sensors, and as bioimaging agents.[1–7] These materials are alternatives to phosphorescent inorganic complexes and offer advantages including synthetic versatility, lower cost, and reduced toxicity. Controllable variation of the photophysical properties such as photoluminescence quantum yield (PLQY) and lifetime of organic luminescent materials is critical to obtain desired characteristics for specific applications. In this work, we use organic alloys to tune these properties.

Organic alloys are homogeneous solid compositions formed by random occupancy of isostructural guest molecules in the crystal lattice of a host compound.[8–10] Compositions can range from 0% to 100% of each of the two components, offering broad and continuous control over material properties.[11] Organic alloys have been utilized to tune optoelectronic behavior and energy levels of organic semiconductors for applications such as organic photovoltaics (OPVs) and organic field-effect transistors (OFETs),[12–15] in addition to adjusting the luminescence properties of organic co-assemblies.[9,10,16] Compositional changes are usually limited due to challenges in preparing organic alloys by crystallization.[9,12,14,17]

In this work, we target two well-known photophysical phenomena, namely room temperature phosphorescence (RTP) and thermally activated delayed fluorescence (TADF) for our initial explorations of organic alloy systems. In RTP,[1–4] photoluminescence may persist even after the photoexcitation source has been removed (so-called afterglow) due to its long lifetime (ms to s). TADF occurs when the singlet–triplet energy gap (ΔE_{ST}) is small (<0.2 eV), and excitons can repopulate the singlet state from triplet states *via* endothermic reverse intersystem crossing (RISC).[18] TADF has been extensively used in OLEDs,[5–7] however it remains challenging to develop TADF emitters with prolonged lifetime and afterglow,[19–21] which would offer interesting opportunities to circumvent non-radiative decay of triplets and enable higher energy afterglow (typically RTP emitters phosphoresce above 500 nm).

Crystallization is usually required to stabilize triplet excitons for organic small molecule RTP emitters, thus prolonging triplet lifetime and enhancing efficiency.[22–31] Another common approach to tuning triplet utilization *via* RTP and TADF in organic materials involves incorporating guest dopants in host matrices at low concentrations in order to modify the photophysical properties.[32–43] Doped host–guest systems in the form of crystals, powders, or films can provide a rigid environment that promotes triplet emission. The concentrations of dopant guest compounds are relatively low (~1 wt%), and increasing the amount of guest to above 10% can result in self-quenching and a decrease in phosphorescence efficiency and lifetime.[34,38] It is also worth noting that when host and guest have strong charge-transfer interactions, organic long persistent

Department of Chemistry, University of British Columbia, 2036 Main Mall, Vancouver, BC, V6T 1Z1, Canada. E-mail: mwolf@chem.ubc.ca

† Electronic supplementary information (ESI) available: Synthetic and computational details. CCDC 2116284–2116290. For ESI and crystallographic data in CIF or other electronic format see https://doi.org/10.1039/d2sc01922a

‡ These authors contributed equally to the work.

luminescence (OLPL) can occur with hours of afterglow emission.[44–46] OLPL differs from TADF and RTP in mechanism.[46]

Host compounds are typically non-emissive and serve as rigid matrices for triplet emission. Co-crystallization of a small percentage of a phosphorescent guest compound with a structurally similar non-emissive host resulted in 20-fold phosphorescence enhancement compared to the pure guest crystal alone.[33] In some cases, interactions between host and guest compounds can lead to charge-separated states to give long-lived phosphorescence.[40] Zhang and co-workers recently developed a doped host–guest system in which TADF was employed to realize both long-lived and efficient afterglow.[47] The Tang group has developed host–guest systems where two emitters were used to enable a triplet energy trap or exciplex, allowing improved triplet efficiency and lifetime.[39,41] Usually not much improvement is observed in lifetime by varying the dopant ratio.[48] The limited compositional ratio range of host and guest compounds leads to limited tunability in lifetime and efficiency.[28]

Using organic alloys to tune TADF or RTP behavior by compositional changes is intriguing, and can potentially provide advantages beyond host–guest systems. Variation of the ratio of crystalline triplet emitters with similar chemical structures in the alloy offers dual tunability of both lifetime and efficiency, a feature that host–guest systems typically fail to offer. In addition, it also helps avoid the self-quenching that is commonly seen in doped host–guest systems at higher concentrations, which enables more compositional tunability than is possible in host–guest systems. The successful design of long-lived triplet luminescent organic alloys requires the two-component compounds to be structurally similar yet have contrasting photophysical properties. Ideally, one component has a higher PLQY and the other a longer emission lifetime, allowing the resulting alloys to potentially exhibit the merits of each compound. If the two compounds are isostructural, alloys can be formed over a large compositional range by recrystallization.

Due to recent progress on molecular design for RTP, we were able to select two reported compounds, (9*H*-carbazol-9-yl)(*p*-tolyl)methanone (**CBZ-Me**), and (4-bromophenyl)(9*H*-carbazol-9-yl)methanone (**CBZ-Br**) as the two alloy components (Fig. 1). **CBZ-Me** is an RTP emitter with 21 ms (@453 nm) and 340 ms (@530 nm) lifetime and a PLQY of 2.00%.[26] **CBZ-Br**, on the other hand, has two polymorphs, referred to as **CBZ-Br** and **CBZ-Br-RTP** (Fig. S2 and Table S1†).[25,49] One polymorph (**CBZ-Br**) is isostructural with **CBZ-Me** and shows TADF, with a delayed lifetime of 3.4 μs and a PLQY of 18.0%. The other polymorph (**CBZ-Br-RTP**) only shows RTP. The difference between **CBZ-Me** and **CBZ-Br** in lifetime and PLQY is presumably the result of the heavy atom effect in **CBZ-Br**, which facilitates RISC, enhancing PLQY and decreasing the delayed lifetime.[50] The methyl group, however, can prolong triplet lifetime by facilitating intermolecular interactions.[24] In this work, we mix **CBZ-Br** and **CBZ-Me** in different ratios to make a series of organic alloys ($\mathbf{Me}_x\mathbf{Br}_{10-x}$, where x = 3 to 10) obtained through recrystallization. This enables fine-tuning of PLQYs and triplet lifetimes and allows dialing in of photophysical properties for specific applications.

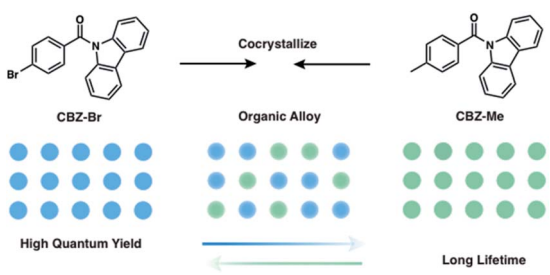

Fig. 1 Chemical structures of parent compound CBZ-Me and CBZ-Br and the design principle of tunable organic alloys.

Crystallography

CBZ-Me and **CBZ-Br** are soluble in acetonitrile across the molar ratio range, allowing the growth of large (~1 mm × ~1 mm × ~1 mm) high-quality alloy crystals ($\mathbf{Me}_x\mathbf{Br}_{10-x}$, where x = 3 to 10) during slow evaporation experiments in this solvent (Fig. S3 and Table S2†). Acetonitrile promoted the crystallization of the **CBZ-Br** polymorph over the **CBZ-Br-RTP** polymorph allowing further access across the molar range by isostructural substitution. Attempts to produce organic alloy crystals with compositions containing **CBZ-Br** percentages higher than 70% were unsuccessful due to **CBZ-Br** crystallizing as a mixture of the **CBZ-Br-RTP** polymorph and alloy crystals with **CBZ-Me** compositions of approximately 30%.

Similar to the crystals of the pure compounds **CBZ-Me** and **CBZ-Br**, the organic alloys are isostructural and crystallize in the $P2_1/n$ space group with one molecule in the asymmetric unit. Crystallographically, the organic alloys are observed as substitutional disorder where the molecules occupy the exact fractional coordinates in the lattice (Fig. S4†), and the methyl and bromide groups are refined using a two-part disorder model (Fig. 2(a)). The site occupancy factors obtained from the crystal structures match the stoichiometric ratios determined by solution ^{1}H NMR spectroscopy upon dissolution of the alloy crystals (Fig. S5 and Table S3†). With an increasing percentage of **CBZ-Me** in the alloy, the unit cell axes remain essentially unchanged with a slight decrease of 0.32° in the β angle tending toward the pure **CBZ-Me** structure (Fig. S6†). The unit cell volume was also found to decrease with increasing **CBZ-Me** percentage as the van der Waals volume of the methyl group occupies 1.53 Å^3 less volume than the bromide group at the *para* position.[51] Furthermore, short-range order (SRO) defects usually occur in disordered materials giving rise to diffuse scattering in addition to Bragg diffraction peaks.[52,53] These organic alloys produce very low-intensity diffuse scattering, indicating that the SRO populations are very low and that the two components are homogenized within the lattice (Fig. S7†).

The homogeneity of the organic alloys was probed by differential scanning calorimetry (DSC) to assess the melting points of the parent compound and crystal alloys (Fig. 2(b)). **CBZ-Br** (TADF polymorph) melts at 156 °C, and with increasing **CBZ-Me** composition, the melting point of the crystal alloys increases with pure **CBZ-Me** melting at 177 °C. The linearity of

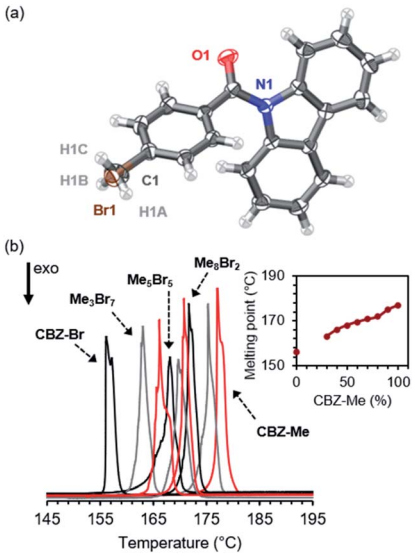

Fig. 2 (a) Representative ORTEP of substitutional disorder for organic alloys (Me_xBr_{10-x}, x = 3 to 10), ellipsoids drawn at 50% probability, hydrogens are plotted as spheres. Only heteroatoms and the methyl group are labelled for clarity. (b) DSC traces of organic alloys (Me_x-Br_{10-x}, x = 3 to 10) where endotherms are labelled with their corresponding composition ratio, Me_4Br_6, Me_6Br_4, Me_9Br_1 labels are excluded for clarity. (Inset: melting point temperatures as a function of CBZ-Me percentage).

the melting point range is consistent with the alloys being comprised of a single-phase system with homogenous distribution of the components in the crystals.[11]

Photophysics

The photophysical properties of the parent compounds **CBZ-Me** and **CBZ-Br** were examined in the single-crystal state. Liu and co-workers have raised the issue that carbazole isomers may induce long-lived phosphorescence.[40] We did not observe any isomers in our recrystallized 9-*H* carbazole starting materials as evaluated by HPLC on the redissolved crystals, and the fluorescence spectra match those of the same compounds prepared by Liu and co-workers. The characteristic fine-structured localized phosphorescence of **CBZ-Me** is no longer observed, and instead, we obtain a broad featureless delayed spectrum, which resembles that of a structurally similar species, (4-chlorophenyl)(9*H*-carbazol-9-yl)methanone **CPhCz** (ESI Fig. 6(c), *Nat. Mater.*, 2020, **14**, 175–180†).[40] This long-lived emission band has a TADF feature at 450 nm with a 38 ms lifetime (Fig. S8†). The delayed lifetime feature is present in more significant amounts at an elevated temperature while the intensity of the emission band below 450 nm gradually increases with increasing temperature. In the low-energy region >500 nm, the long-lived emission shows a much longer lifetime >300 ms, which can be assigned as RTP. The long-lived emission feature of **CBZ-Me** is present at relatively low amplitude compared to prompt fluorescence.

CBZ-Br gives a similar microsecond delayed lifetime to that previously reported for this compound.[43] A long-lived TADF feature was also observed with a lifetime of 76.3 ms, confirmed by the spectral overlap between the steady-state emission and the delayed photoluminescence at 1 ms (Fig. S9†). Similarly, in the lower-energy region, the lifetime of **CBZ-Br** is prolonged to 143 ms. Due to the long lifetimes, the delayed photoluminescence spectrum of this prolonged feature could not be accurately measured. **CBZ-Br** likely has a 'hidden' RTP state that can preserve triplet excitons for long-lived TADF emission and yield a longer lifetime above 500 nm.[54]

PLQY values of both parent compounds (44.0% for **CBZ-Br** and 11.8% for **CBZ-Me**) are greater than reported in the literature, possibly due to sample crystallinity or instrumental differences. We speculate that the lifetime and PLQY differences between **CBZ-Me** and **CBZ-Br** result from the heavy atom effect in **CBZ-Br**, which facilitates RISC and promotes TADF over RTP, enhancing RISC PLQY and resulting in a decrease in RTP lifetime. The methyl group facilitates improved molecular packing, which can prolong the RTP lifetime.[24]

Steady-state and time-gated photoluminescence measurements were carried out on the alloy crystals. The steady-state emission maxima of the alloys are between those of the parent compounds (475 and 453 nm, respectively, for **CBZ-Br** and **CBZ-Me**), shifting slightly towards higher energy with increasing **CBZ-Me** composition (Fig. 3(a) and S10†). The time-gated spectra (1 ms delay) of the alloys are almost identical for all ratios, showing broad emission with maxima of 475 nm. Overall, they overlap well with the steady-state spectra, with slight differences observed in alloys with high **CBZ-Me** ratios. All the alloy crystals display prompt and delayed emission in their photoluminescence decays (Fig. 3(b)). The alloy crystal with the highest percentage of **CBZ-Br**, $\mathbf{Me_3Br_7}$, shows the shortest delayed lifetime of 107 ms, which is still a 1.5-fold and 3-fold enhancement compared to **CBZ-Br** (76.3 ms), and **CBZ-Me** (@450 nm) (37.8 ms) delayed lifetimes, respectively. The amplitude of the delayed component is much larger than in the parent compounds. $\mathbf{Me_9Br_1}$, on the other hand, shows an increase in lifetime (197 ms) by a factor of 2 compared to $\mathbf{Me_3Br_7}$, while the delayed lifetimes of other alloys lie between $\mathbf{Me_3Br_7}$ and $\mathbf{Me_9Br_1}$.

When photoluminescence decays of the alloys were collected at 550 nm at room temperature, tails of longer decays were found with about 10% amplitude (Fig. S19†). The lifetimes of the alloys fall between those of **CBZ-Br** (143 ms) and **CBZ-Me** (404 ms) at 550 nm. Due to their low amplitudes and long lifetimes, the time-resolved spectra of these features could not be separated from the dominant delayed emission feature. However, we speculate they might originate from the RTP states of **CBZ-Me** and **CBZ-Br**. These results demonstrate that emission lifetime can be enhanced and systematically tuned by changing the compositional ratios of two parent compounds in alloy crystals.

The photoluminescence quantum yields of the alloys fall in the range between the two parent compounds. Generally, higher **CBZ-Br** content results in higher luminescence efficiency, which is the opposite of the observed trend in lifetimes. For example, $\mathbf{Me_3Br_7}$ has a PLQY of 26.7%, while $\mathbf{Me_9Br_1}$ shows only 14.0% efficiency. A digital single-lens camera was used to capture the

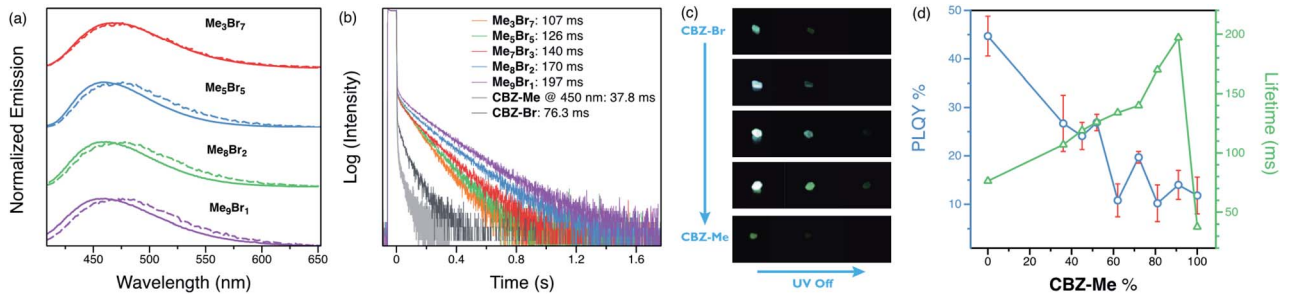

Fig. 3 (a) Steady-state (solid line) and 1 ms delay (dashed line) photoluminescence spectra of organic alloys (spectra of Me_4Br_6, Me_6Br_4, and Me_7Br_3 have been omitted for the clarity of the figure). (b) Phosphorescence decay of organic alloys and parent compound **CBZ-Me** crystals under air at room temperature (decay traces of Me_4Br_6, Me_6Br_4 have been omitted for clarity). (c) Photos of **CBZ-Br**, Me_3Br_7, Me_5Br_5, Me_9Br_1, and **CBZ-Me** upon removal of UV excitation. (d) Plots of PLQYs and delayed lifetimes against **CBZ-Me** ratios.

afterglow of alloy crystals after removing UV excitation (Fig. 3(c)). Even though parent compound **CBZ-Br** has the highest overall luminescence efficiency and **CBZ-Me** displays the most extended RTP lifetime, the afterglow from the parent compounds is relatively weak and short, which can be attributed to the short delayed lifetime of **CBZ-Br** and the faint luminescence of **CBZ-Me**, in addition to the low amplitudes of long-lived species.

On the other hand, the alloy crystals emit much more intense long-lived emission, and increasing the percentage of **CBZ-Me** results in a slightly longer afterglow. Hence, it can be concluded that these organic alloys provide a wide range of tunability of both lifetime and efficiency with compositional ratio changes (Fig. 3(d)). It is possible to choose a ratio that results in either more emissive or longer-lived materials, depending on the desired properties for particular applications. Variable-temperature experiments were carried out to help elucidate the origin of the delayed emission. For Me_5Br_5, at temperatures below 200 K, structured emission peaks at 485 and 517 nm were observed, while emission >460 nm is much weaker in intensity. When the temperature is increased, the fine-structured band decreases dramatically and eventually becomes structureless. The vibronic character and temperature-dependence of the emission confirm that the phosphorescence arises from a locally excited state, not due to carbazole isomers at low temperature (Fig. 4(a) and S13–S18†).[21,26,55] A broad emission band peaking at ~460 nm starts growing with increasing temperature. The photoluminescence decay curves exhibit increasing amplitudes of the delayed features with shortened delayed lifetimes at elevated temperatures (Fig. 3(b)).

The excited-state pathways of the parent compounds are quite different from each other (Fig. 4(c)). **CBZ-Br** displays two RISC channels with distinct timescales (μs and ms), possibly originating from different triplet excited states.[50] As a result, TADF is the major radiative pathway besides prompt fluorescence, resulting in a high PLQY. Even though the RTP state exists in **CBZ-Br**, it is overshadowed by strong TADF, as indicated by the well-overlapped steady-state and delayed spectra.[54] On the other hand, **CBZ-Me** only exhibits slow RISC, and RTP is the dominant triplet radiative pathway, which leads to reduced emission efficiency. However, triplet excited states can function as traps and therefore give a longer lifetime.[26] Since the two parent compounds exhibit identical packing modes and singlet–triplet energy gaps (~0.2 eV), indicated by low-temperature measurements (Fig. S8 and S9†), it can be deduced that the electronic effects of the bromide and methyl groups are the main reason for the differences. The Br group is responsible for facilitating RISC[50] while the methyl group results in the long-lived triplet excited state. When the two species are mixed to form alloys, the fast RISC channel is entirely suppressed by methyl involvement (Table S3 and Fig. S11(d)†). However, long-lived triplet states preserve the triplet exciton, followed by slow RISC facilitated by the Br group to emit TADF. Even though the PLQYs, as well as lifetimes above 550 nm, show almost linear changes by compositional variations, the fact that TADF lifetimes increase 1.5-fold (compared to **CBZ-Br**) to 5-fold (compared to **CBZ-Me**), proves the existence of interactions between two parent species. Mechanisms such

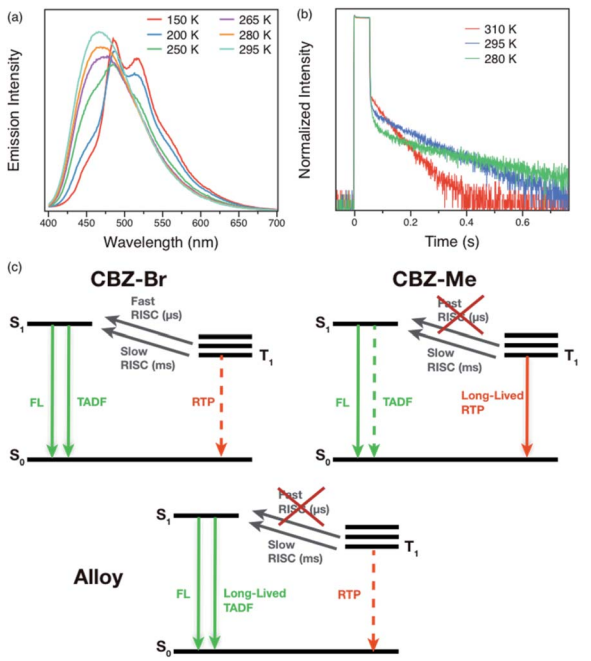

Fig. 4 Variable-temperature (a) steady-state photoluminescence spectra and (b) phosphorescence decays of Me_5Br_5 under helium atmosphere. (c) Jablonski diagrams of parent compounds and Me_5Br_5.

as energy transfer or charge separation and recombination can be ruled out since the two-parent compounds share similar absorption spectra and oxidation potentials (Fig. S21†) due to their similar structure.

Conclusions

In conclusion, **CBZ-Me** and **CBZ-Br** have been crystallized together in various ratios to yield seven crystalline organic alloys ($\mathbf{Me}_x\mathbf{Br}_{10-x}$, where $x = 3$ to 10). This is the first report employing organic alloys as long-lived emissive materials. The alloys exhibit long-lived TADF that gives strong afterglow emission, and TADF lifetimes show 1.5-fold (compared to **CBZ-Br**) to 5-fold (compared to **CBZ-Me**) enhancement compared to parent compounds. The compositional change offers broad tunability in both lifetime and PLQYs, which addresses the trade-off between efficiency and lifetime.

Organic RTP and TADF materials have been of intense interest over the last few years, and several design principles for small molecules offering these characteristics have been established. With a rich library of emitters in hand, we believe that organic alloys provide an exciting opportunity to utilize existing molecular emitters to achieve better overall luminescence performance, promoting the development of RTP and TADF materials.

In addition, tremendous effort has been made towards altering long-lived luminescent properties by variations of host and guest compounds. In this work, we put forward an alternative strategy, organic alloys, to control photoluminescent properties by varying compositional ratios. Organic alloys minimize self-quenching using crystalline triplet emitters, thus providing a more comprehensive range of tunability over luminescence properties than the commonly used host–guest systems. Furthermore, this has the potential to be expanded into multi-component systems or to be used in combination with host–guest systems, which will offer numerous opportunities in both material design and practical applications.

Author contributions

Z. X. and D. H. contributed equally to this work. Z. X. conceived the idea and conducted steady-state and time-gated photoluminescence measurements. D. H. conducted the XRD and DSC measurements. J. Y. performed the photoluminescence quantum yield measurements. M. O. W. provided guidance throughout the project. All authors contributed to the writing of the manuscript.

Conflicts of interest

There are no conflicts of interest to declare.

Acknowledgements

We acknowledge the Natural Sciences and Engineering Research Council of Canada (NSERC) for funding, Dr J. F. Britton, MAX Diffraction Facility, Department of Chemistry, McMaster University for diffuse X-ray diffraction experiments and interpretation of the data, and the Laboratory for Advanced Spectroscopy and Imaging Research (LASIR) for facility access. We would like to thank Dr Saeid Kamal for his assistance with spectroscopic studies.

Notes and references

1 Kenry, C. Chen and B. Liu, *Nat. Commun.*, 2019, **10**, 2111.
2 Q. Li, Y. Tang, W. Hu and Z. Li, *Small*, 2018, **14**, 1801560.
3 A. Forni, E. Lucenti, C. Botta and E. Cariati, *J. Mater. Chem. C*, 2018, **6**, 4603–4626.
4 W. Zhao, Z. He and B. Z. Tang, *Nat. Rev. Mater.*, 2020, **5**, 869–885.
5 Z. Yang, Z. Mao, Z. Xie, Y. Zhang, S. Liu, J. Zhao, J. Xu, Z. Chi and M. P. Aldred, *Chem. Soc. Rev.*, 2017, **46**, 915–1016.
6 Y. Liu, C. Li, Z. Ren, S. Yan and M. R. Bryce, *Nat. Rev. Mater.*, 2018, **3**, 18020.
7 M. Godumala, S. Choi, M. J. Cho and D. H. Choi, *J. Mater. Chem. C*, 2019, **7**, 2172–2198.
8 E. M. Engler, B. A. Scott, S. Etemad, T. Penney and V. V. Patel, *J. Phys. Chem.*, 1977, **99**, 5909–5916.
9 Y. Lei, Y. Sun, Y. Zhang, H. Zhang, H. Zhang, Z. Meng, W. Y. Wong, J. Yao and H. Fu, *Nat. Commun.*, 2018, **9**, 4358.
10 H. Zhang, H. Wang, P.-C. Qian and W. Y. Wong, *Nanoscale*, 2020, **12**, 16414–16419.
11 M. Dabros, P. R. Emery and V. R. Thalladi, *Angew. Chem., Int. Ed.*, 2007, **46**, 4132–4135.
12 Y. Zhen, H. Tanaka, K. Harano, S. Okada, Y. Matsuo and E. Nakamura, *J. Am. Chem. Soc.*, 2015, **137**, 2247–2252.
13 X. Xu, T. Xiao, X. Gu, X. Yang, S. V. Kershaw, N. Zhao, J. Xu and Q. Miao, *ACS Appl. Mater. Interfaces*, 2015, **7**, 28019–28026.
14 J.-H. Dou, Z.-A. Yu, J. Zhang, Y.-Q. Zheng, Z.-F. Yao, Z. Tu, X. Wang, S. Huang, C. Liu, J. Sun, Y. Yi, X. Cao, Y. Gao, J.-Y. Wang and J. Pei, *J. Am. Chem. Soc.*, 2019, **141**, 6561–6568.
15 X. Huang, X. Liu, K. Ding and S. R. Forrest, *Mater. Horiz.*, 2020, **7**, 244–251.
16 Y.-Q. Sun, Y.-L. Lei, X.-H. Sun, S.-T. Lee and L.-S. Liao, *Chem. Mater.*, 2015, **27**, 1157–1163.
17 R. Natarajan, G. Magro, L. N. Bridgland, A. Sirikulkajorn, S. Narayanan, L. E. Ryan, M. F. Haddow, A. G. Orpen, J. P. H. Charmant, A. J. Hudson and A. P. Davis, *Angew. Chem., Int. Ed.*, 2011, **50**, 11386–11390.
18 F. B. Dias, T. J. Penfold and A. P. Monkman, *Methods Appl. Fluoresc.*, 2017, **5**, 012001.
19 J. Chen, T. Yu, E. Ubba, Z. Xie, Z. Yang, Y. Zhang, S. Liu, J. Xu, M. P. Aldred and Z. Chi, *Adv. Opt. Mater.*, 2019, **7**, 1801593.
20 J.-X. Wang, Y.-G. Fang, C.-X. Li, L.-Y. Niu, W.-H. Fang, G. Cui and Q. Z. Yang, *Angew. Chem., Int. Ed.*, 2020, **59**, 10032–10036.
21 Z. Mao, Z. Yang, C. Xu, Z. Xie, L. Jiang, F. L. Gu, J. Zhao, Y. Zhang, M. P. Aldred and Z. Chi, *Chem. Sci.*, 2019, **10**, 7352–7357.

22 Y. Xiong, Z. Zhao, W. Zhao, H. Ma, Q. Peng, Z. He, X. Zhang, Y. Chen, X. He, J. W. Y. Lam and B. Z. Tang, *Angew. Chem., Int. Ed.*, 2018, **57**, 7997–8001.
23 N. Gan, X. Wang, H. Ma, A. Lv, H. Wang, Q. Wang, M. Gu, S. Cai, Y. Zhang, L. Fu, M. Zhang, C. Dong, W. Yao, H. Shi, Z. An and W. Huang, *Angew. Chem., Int. Ed.*, 2019, **58**, 14140–14145.
24 Z. Mao, Z. Yang, Z. Fan, E. Ubba, W. Li, Y. Li, J. Zhao, Z. Yang, M. P. Aldred and Z. Chi, *Chem. Sci.*, 2019, **10**, 179–184.
25 S. Cai, H. Shi, J. Li, L. Gu, Y. Ni, Z. Cheng, S. Wang, W. W. Xiong, L. Li, Z. An and W. Huang, *Adv. Mater.*, 2017, **29**, 1701244.
26 Y. Xie, Y. Ge, Q. Peng, C. Li, Q. Li and Z. Li, *Adv. Mater.*, 2017, **29**, 1606829.
27 Z. Xu, C. Climent, C. M. Brown, D. Hean, C. J. Bardeen, D. Casanova and M. O. Wolf, *Chem. Sci.*, 2021, **12**, 188–195.
28 Y. Shoji, Y. Ikabata, Q. Wang, D. Nemoto, A. Sakamoto, N. Tanaka, J. Seino, H. Nakai and T. Fukushima, *J. Am. Chem. Soc.*, 2017, **139**, 2728–2733.
29 W. Ye, H. Ma, H. Shi, H. Wang, A. Lv, L. Bian, M. Zhang, C. Ma, K. Ling, M. Gu, Y. Mao, X. Yao, C. Gao, K. Shen, W. Jia, J. Zhi, S. Cai, Z. Song, J. Li, Y. Zhang, S. Lu, K. Liu, C. Dong, Q. Wang, Y. Zhou, W. Yao, Y. Zhang, H. Zhang, Z. Zhang, X. Hang, Z. An, X. Liu and W. Huang, *Nat. Mater.*, 2021, **20**, 1539–1544.
30 Z. Yuan, J. Wang, L. Chen, L. Zou, X. Gong and X. Ma, *CCS Chem.*, 2020, **2**, 158–167.
31 L. Bian, H. Shi, X. Wang, K. Ling, H. Ma, M. Li, Z. Cheng, C. Ma, S. Cai, Q. Wu, N. Gan, X. Xu, Z. An and W. Huang, *J. Am. Chem. Soc.*, 2018, **140**, 10734–10739.
32 S. Guo, W. Dai, X. Chen, Y. Lei, J. Shi, B. Tong, Z. Cai and Y. Dong, *ACS Mater. Lett.*, 2021, **3**, 379–397.
33 O. Bolton, K. Lee, H.-J. Kim, K. Y. Lin and J. Kim, *Nat. Chem.*, 2011, **3**, 205–210.
34 O. Bolton, D. Lee, J. Jung and J. Kim, *Chem. Mater.*, 2014, **26**, 6644–6649.
35 D. Lee, O. Bolton, B. C. Kim, J. H. Youk, S. Takayama and J. Kim, *J. Am. Chem. Soc.*, 2013, **135**, 6325–6329.
36 M. S. Kwon, D. Lee, S. Seo, J. Jung and J. Kim, *Angew. Chem., Int. Ed.*, 2014, **53**, 11177–11181.
37 S. Hirata, K. Totani, J. Zhang, T. Yamashita, H. Kaji, S. R. Marder, T. Watanabe and C. Adachi, *Adv. Funct. Mater.*, 2013, **23**, 3386–3397.
38 N. Notsuka, R. Kabe, K. Goushi and C. Adachi, *Adv. Funct. Mater.*, 2017, **27**, 1703902.
39 X. Zhang, L. Du, W. Zhao, Z. Zhao, Y. Xiong, X. He, P. F. Gao, P. Alam, C. Wang, Z. Li, J. Leng, J. Liu, C. Zhou, J. W. Y. Lam, D. L. Phillips, G. Zhang and B. Z. Tang, *Nat. Commun.*, 2019, **10**, 5161.
40 C. Chen, Z. Chi, K. C. Chong, A. S. Batsanov, Z. Yang, Z. Mao, Z. Yang and B. Liu, *Nat. Mater.*, 2020, **14**, 175–180.
41 Y. Wang, H. Gao, J. Yang, M. Fang, D. Ding, B. Z. Tang and Z. Li, *Adv. Mater.*, 2021, **33**, 2007811.
42 L. Ma, Q. Xu, S. Sun, B. Ding, Z. Huang, X. Ma and H. Tian, *Angew. Chem., Int. Ed.*, 2022, **61**, e202115748.
43 B. Ding, L. Ma, Z. Huang, X. Ma and H. Tian, *Sci. Adv.*, 2021, **7**, eabf9668.
44 R. Kabe and C. Adachi, *Nature*, 2017, **550**, 384–387.
45 P. Alam, N. L. C. Leung, J. Liu, T. S. Cheung, X. Zhang, Z. He, R. T. K. Kwok, J. W. Y. Lam, H. H. Y. Sung, I. D. Williams, C. C. S. Chan, K. S. Wong, Q. Peng and B. Z. Tang, *Adv. Mater.*, 2020, **32**, 2001026.
46 Z. Lin, R. Kabe, K. Wang and C. Adachi, *Nat. Commun.*, 2020, **11**, 191.
47 X. Wang, Y. Sun, G. Wang, J. Li, X. Li and K. Zhang, *Angew. Chem., Int. Ed.*, 2021, **60**, 17138–17147.
48 B. Chen, W. Huang, X. Nie, F. Liao, H. Miao, X. Zhang and G. Zhang, *Angew. Chem., Int. Ed.*, 2021, **60**, 16970–16973.
49 Y. Liu, G. Zhan, P. Fang, Z. Liu, Z. Bian and C. Huang, *J. Mater. Chem. C*, 2017, **5**, 12547–12552.
50 Z. Xu, D. Hean, C. Climent, D. Casanova and M. O. Wolf, *Mater. Adv.*, 2021, **2**, 5777–5784.
51 A. Bondi, *J. Org. Chem.*, 1964, **68**, 441–451.
52 T. R. Welberry, R. L. Withers and J. C. Osborn, *Acta Crystallogr.*, 1990, **46**, 267–275.
53 T. R. Welberry and B. D. Butler, *Chem. Rev.*, 1995, **95**, 2369–2403.
54 X. Cai, Z. Qiao, M. Li, X. Wu, Y. He, X. Jiang, Y. Cao and S.-J. Su, *Angew. Chem., Int. Ed.*, 2019, **58**, 13522–13531.
55 H. Zhu, I. Badía-Domínguez, B. Shi, Q. Li, P. Wei, H. Xing, M. C. R. Delgado and F. Huang, *J. Am. Chem. Soc.*, 2021, **143**, 2164–2169.